Nonresonant EUV-UV two-color two-photon ionization of He studied by single-shot photoelectron spectroscopy

M. Fushitani,[1,2] Y. Hikosaka,[2,3] A. Matsuda,[1] T. Endo,[1] E. Shigemasa,[2,4] M. Nagasono,[2] T. Sato,[2] T. Togashi,[5] M. Yabashi,[2,5] T. Ishikawa,[2] and A. Hishikawa[1,2,*]

[1]*Department of Chemistry, Graduate School of Science, Nagoya University, Nagoya, Aichi 464-8602, Japan*
[2]*RIKEN, SPring-8 Center, Sayo, Hyogo 679-5148, Japan*
[3]*Department of Environmental Science, Faculty of Science, Niigata University, Niigata, Niigata 950-2181, Japan*
[4]*Institute for Molecular Science, National Institutes of Natural Sciences, Myodaiji, Okazaki, Aichi 444-8585, Japan*
[5]*Japan Synchrotron Radiation Research Institute, Sayo, Hyogo 679-5198, Japan*

(Received 26 September 2013; published 31 December 2013)

Single-shot photoelectron spectroscopy of nonresonant two-color two-photon ionization of He has been carried out using an intense free-electron laser (FEL) at 59.7 nm and a femtosecond UV laser at 268 nm. By shot-by-shot analysis of photoelectron spectra, the cross section for nonresonant two-color ionization of He is determined to be $\sigma^{(2)} = 4.1(6) \times 10^{-52}$ cm^4 s. The cross-correlation trace derived from the nonresonant signals shows that the temporal resolution of the system is 0.36(3) ps, which is mainly governed by the timing jitter between the FEL and UV laser pulses.

DOI: 10.1103/PhysRevA.88.063422 PACS number(s): 32.80.Fb, 32.80.Rm, 32.80.Wr

I. INTRODUCTION

Nonlinear phenomena of atoms in intense extreme ultraviolet (EUV) and x-ray laser fields have been subjected to intensive studies in recent years [1–3], along with the recent advances in free-electron laser (FEL) technology in this short wavelength region. Two-photon ionization of He has been investigated in detail both experimentally using FEL [4–6] or laser high-order harmonics [7–9] and theoretically [10–16]. For example, one-color two-photon ionization has been studied with photon energies below the ionization threshold (24.59 eV) by using ion spectrometry at four different FEL wavelengths at around the $2\,^1P$-$1\,^1S$ resonance (58.4 nm) [6].

Free-electron lasers operated in the self-amplified spontaneous emission (SASE) scheme fluctuate both in wavelength and intensity due to the statistical nature of the spontaneous emission. The shot-to-shot fluctuation often blurs details of the nonlinear process such as resonances to intermediate states. In recent publications, we have demonstrated that shot-by-shot photoelectron spectroscopy is powerful in experimentally addressing the problem [17–19]. The single-shot spectral measurement, which allows us to determine spectral properties of each FEL pulse and the target response, provides a unique approach to utilizing the pulse-to-pulse fluctuation to clarify the pathways of nonlinear multiphoton ionization of Ar [17,19] and He [18,20] in intense EUV-FEL fields. Here we apply this approach to two-color (EUV-UV) two-photon ionization of He by using a femtosecond UV laser synchronized with a FEL to evaluate the cross sections for resonant and nonresonant nonlinear ionization via the $2\,^1P$ state. By employing a shot-by-shot analysis we evaluate the absolute cross section of nonresonant two-color two-photon ionization in a more accurate way than that by simple ion detection.

The present paper is organized as follows. After describing the experimental setup and the method of data analysis, we first discuss EUV one-color two-photon ionization of He at the $2\,^1P$-$1\,^1S$ resonance by comparison with the previous studies. Then, we discuss EUV-UV nonresonant two-color two-photon ionization of He in detail by using shot-by-shot analysis of photoelectron spectra.

II. EXPERIMENT

The experiment was performed using the SPring-8 Compact SASE Source (SCSS) test accelerator facility at RIKEN Harima [1,21]. The schematic of the experimental setup is shown in Fig. 1(a). Ultrashort intense EUV pulses (∼100 fs, ∼20 μJ) tunable in the wavelength region of 50–61 nm were focused by elliptical and cylindrical mirrors (EM and CM). The focal spot size at the interaction region in the detection chamber was about 25 μm in diameter. The throughput of the optical system was about 35%. The mean pulse energy of the FEL was controlled by using an Ar gas attenuator placed in the upper stream of the beamline. Ultrafast UV laser pulses (∼100 fs) generated from a femtosecond Ti:Sa laser system with a frequency converter unit were introduced by using a plano-convex lens (L, $f = 1000$ mm) and a steering mirror (SM) to the interaction region at an angle of ∼1° with respect to the FEL pulses. Both FEL and UV laser pulses were horizontally polarized. The mean time delay between the FEL and optical laser pulses was controlled by an optical delay-line stage with a 1 μm resolution.

The experiment was performed using He and Ar as the target. They were introduced into the vacuum chamber (base pressure 2.6×10^{-7} Pa) through separate capillaries to control the partial pressures independently. The gas pressures were measured by using a combination gauge (Anelva, M-336MX) with the relative sensitivity factor being 0.2 for He and 1.2 for Ar. The local gas density at the laser focus is calibrated for each capillary. Photoelectrons produced by the FEL and/or optical laser pulses were detected on the shot-by-shot basis by using a magnetic bottle-type photoelectron spectrometer. The broad background observed without the sample gas was subtracted from the spectra. The energy resolution was estimated to be

*hishi@chem.nagoya-u.ac.jp

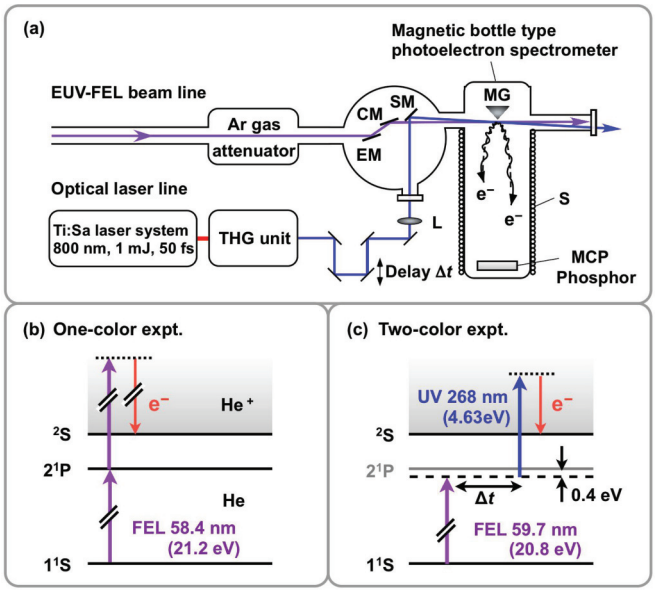

FIG. 1. (Color online) (a) Experimental setup. The EUV-FEL beamline includes an Ar gas attenuator for the FEL intensity monitor, a mirror system consisting of elliptical (EM) and cylindrical (CM) mirrors for focusing, and a magnetic bottle-type photoelectron spectrometer. The magnetic mirror formed by a permanent magnet (MG) and a solenoid (S) directs all the photoelectrons to a microchannel plate (MCP) with a phosphor screen. An ultrashort laser pulse from the optical laser line is introduced with a certain time delay Δt into the spectrometer and coupled with FEL pulses with an angle of $\sim 1^\circ$ by a steering mirror (SM) inside the FEL beamline. The time delay between the FEL and optical laser pulses is controlled by an optical delay-line stage. (b) One-color two-photon ionization via the He $2\,^1P$ state by EUV FEL at 58.4 nm (21.2 eV). (c) Two-color two-photon ionization with EUV FEL at 59.7 nm (20.8 eV) and UV pulses at 268 nm (4.63 eV).

$E/\Delta E = 20$ for photoelectron energies $E < 100$ eV under present conditions. The photoelectron energy was calibrated by the autoionization peaks of O^* atoms produced from O_2^* [22] and the Auger electrons of Xe [23] using the third-order harmonics of FEL [17].

III. DATA ANALYSIS USING KINETIC MODEL

A. Kinetic model

The rate equation for two-photon ionization of He may be written as [24,25]

$$\frac{dn_{\mathrm{He}^+}(t)}{dt} = n_{\mathrm{He}}(t)\sigma^{(2)}_{\mathrm{He}}(h\nu_i,h\nu_j)\frac{I_i(t)}{h\nu_i}\frac{I_j(t-\Delta t)}{h\nu_j}, \quad (1)$$

where $n_{\mathrm{He}}(t)$ and $n_{\mathrm{He}^+}(t)$ represent the number densities of He in the neutral and ionic states at time t, $\sigma^{(2)}_{\mathrm{He}}(h\nu_i,h\nu_j)$ is the two-photon ionization cross section, $I_i(t)$ and $I_j(t)$ are the field intensities of the two laser pulses with photon energies $h\nu_i$ and $h\nu_j$, and Δt is the time delay between these two laser pulses, i and j (=UV, EUV). The number density of He^+ after the laser-pulse interaction may be obtained by integrating Eq. (1) with respect to time t as

$$n_{\mathrm{He}^+}(\infty) = n^0_{\mathrm{He}}\left\{1-\exp\left[-\sigma^{(2)}_{\mathrm{He}}(h\nu_i,h\nu_j)\right]\times\left(\frac{I_{0,i}}{h\nu_i}\right)\left(\frac{I_{0,j}}{h\nu_j}\right)T^{(2)}_{i,j}(\Delta t)\right\}, \quad (2)$$

$$T^{(2)}_{i,j}(\Delta t) = \int_{-\infty}^{+\infty} f_i(t)f_j(t-\Delta t)dt. \quad (3)$$

Here, n^0_{He} is the initial number density of He. The laser field intensity is expressed as $I_i(t) = I_{0,i}f_i(t)$, where $I_{0,i}$ is the peak laser field intensity and $f_i(t)$ is the corresponding pulse envelope normalized at the peak. The photoelectron signal intensity in this two-photon ionization may be written as $S^{(2)}_{\mathrm{He}^+} = \epsilon n_{\mathrm{He}^+}(\infty)$, where ϵ is the overall detection efficiency of the photoelectron spectrometer. When the laser field intensity is well below the saturation limit, $S^{(2)}_{\mathrm{He}^+}$ may be expressed as

$$S^{(2)}_{\mathrm{He}^+} = \epsilon n^0_{\mathrm{He}}\sigma^{(2)}_{\mathrm{He}}(h\nu_i,h\nu_j)\left(\frac{I_{0,i}}{h\nu_i}\right)\left(\frac{I_{0,j}}{h\nu_j}\right)T^{(2)}_{i,j}(\Delta t). \quad (4)$$

The photoelectron signal intensity for single-photon ionization of Ar may be obtained by a similar procedure as

$$S^{(1)}_{\mathrm{Ar}^+} = \epsilon n^0_{\mathrm{Ar}}\sigma^{(1)}_{\mathrm{Ar}}(h\nu_i)\left(\frac{I_{0,i}}{h\nu_i}\right)T^{(1)}_i, \quad (5)$$

$$T^{(1)}_i = \int_{-\infty}^{+\infty} f_i(t)dt, \quad (6)$$

where $\sigma^{(1)}_{\mathrm{Ar}}(h\nu_i)$ is the single-photon ionization cross section of Ar.

In this study, we estimate the two-photon ionization cross section of He, $\sigma^{(2)}_{\mathrm{He}}(h\nu_i,h\nu_j)$, by using the single-photon ionization cross section of Ar, $\sigma^{(1)}_{\mathrm{Ar}}(h\nu_i)$, as a reference. By taking the ratio of photoelectron signal intensity for He^+ [Eq. (4)] with that for Ar^+ [Eq. (5)], the two-photon cross section can be expressed as

$$\sigma^{(2)}_{\mathrm{He}}(h\nu_i,h\nu_j) = \frac{S^{(2)}_{\mathrm{He}^+}}{S^{(1)}_{\mathrm{Ar}^+}}\frac{n^0_{\mathrm{Ar}}}{n^0_{\mathrm{He}}}\frac{T^{(1)}_i}{T^{(2)}_{i,j}(\Delta t)}\frac{h\nu_j}{I_{0,j}}\sigma^{(1)}_{\mathrm{Ar}}(h\nu_i), \quad (7)$$

In the following discussion, the UV pulse is assumed to be Gaussian with a pulse duration of 100 fs. The envelope of fluctuating SASE FEL pulses, $f_{\mathrm{EUV}}(t)$, was simulated by the partial-coherence method [26], where the averaged pulse envelope $\bar{f}_{\mathrm{EUV}}(t)$ was set to be a 100-fs Gaussian.

B. Application to EUV one-color two-photon ionization at 21.2 eV

We first discuss one-color two-photon ionization of He, enhanced by resonance to the $2\,^1P$-$1\,^1S$ transition at 58.4 nm ($h\nu = 21.2$ eV) [see Fig. 1(b)]. Figure 2(a) shows the averaged photoelectron spectrum of the He and Ar gas mixture at the FEL field intensity of 3×10^{12} W/cm^2. The peak observed at 18 eV is due to electrons produced by two-photon ionization of He, while the peak at 5.6 eV is due to single-photon ionization

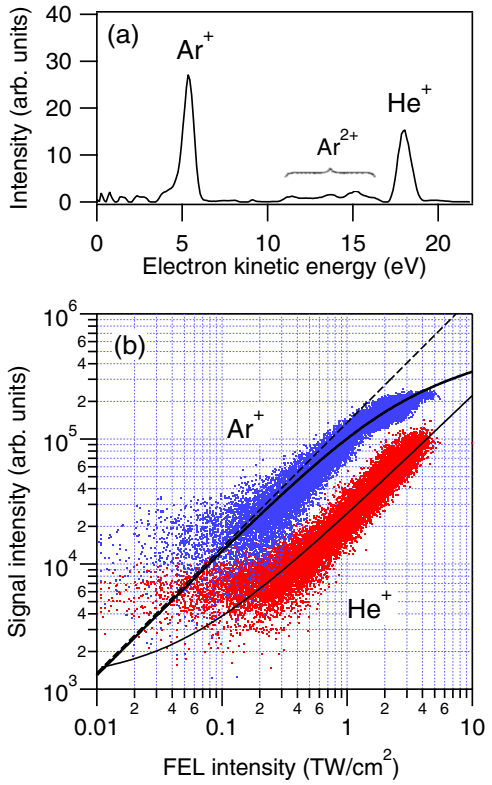

FIG. 2. (Color online) (a) Photoelectron spectrum of He-Ar gas mixture at $h\nu = 21.2$ eV, obtained by averaging over 2×10^3 single-shot photoelectron spectra. The FEL field intensity is $\sim 3 \times 10^{12}$ W/cm^2. The number density ratio between He and Ar is $n^0_{\rm Ar}/n^0_{\rm He} = 3.3 \times 10^{-3}$. (b) Ar^+ (upper) and He^+ (lower) photoelectron intensities plotted against the FEL field intensity. The Ar^+ signals are multiplied by a factor of 1.5 for clarity. The result of the least-squares fitting of He^+ signals is also shown (thin solid line). The deviation from a linear dependence (broken line) observed for Ar^+ at high FEL intensities is well explained by a simulation incorporating the volume effect and the depletion of the ground state (thick solid line).

of Ar. Broad peaks observed in the region of 11–16 eV are assigned to three-photon double ionization of Ar [17,19].

Figure 2(b) plots the He^+ photoelectron yield against the FEL field intensity, obtained by the shot-by-shot analysis of the photoelectron spectra. To cover the wide intensity range, the photoelectron spectra were recorded at different FEL intensities by using the Ar gas attenuator. The data points are distributed along a straight line at high laser field intensities ($\geqslant 1$ TW/cm^2), while they show contributions from a background at small FEL intensities. The background is attributed to the second-order harmonics of FEL, which is not attenuated by the gas attenuator in the present Ar gas pressure range. The least-squares fitting to a power function I^k of the FEL intensity I with a constant background shows that the He^+ yield depends almost linearly [$k = 0.96(1)$] on the fundamental FEL intensity (see Fig. 2). The observed linear dependence is consistent with the previous experimental [6] and theoretical [13,16] studies, showing the significance of the strong single-photon interaction between the ground state and the $1s2p$ state.

It is clearly seen in Fig. 2(b) that the Ar^+ photoelectron signals recorded simultaneously show a clear saturation behavior in the same FEL intensity range, due to the depletion of the ground state Ar by one-photon ionization. The dependence curve is well reproduced by the rate-equation simulation incorporating the nonuniform distribution of the laser field intensity at the focal spot ("volume effect") [17], as shown in Fig. 2(b). A Gaussian radial profile is adopted for the laser field intensity distribution at the focal spot [1]. Since the Rayleigh length ($\sim$12 mm) is sufficiently longer than the size of the detection volume along the beam axis ($\sim$1 mm), the intensity distribution is assumed to be cylindrically symmetric in the simulation. The obtained curve reproduces well the observed Ar^+ signal distribution, and approaches a linear line at the lowest limit in Fig. 2(b) ($\sim 1 \times 10^{11}$ W/cm^2) as expected from Eq. (5). The signal intensity $S^{(1)}_{\rm Ar^+}$, required to evaluate the two-photon cross section [see Eq. (7)], is obtained by extrapolation from the linear region (broken line).

By using the ratio of the signal intensities, $S^{(2)}_{\rm He^+}$ and $S^{(1)}_{\rm Ar^+}$, thus obtained, and the number density ratio estimated from the partial pressures of each gas $n^0_{\rm Ar}/n^0_{\rm He} = 3.3 \times 10^{-3}$, the ratio of the pulse integrals, $T^{(1)}_{\rm EUV}/T^{(2)}_{\rm EUV,EUV}(0) = 1.4$, the one-photon absorption cross section of Ar, $\sigma^{(1)}_{\rm Ar}$ (21.2 eV) $= 3.64 \times 10^{-17}$ cm^2 [27], we obtain $\sigma^{(2)}_{\rm He}$ (21.2 eV, 21.2 eV) $= 5(1) \times 10^{-50}$ cm^4 s at 3×10^{12} W/cm^2. The linear dependence of the He^+ signal (see Fig. 2) suggests that the two-photon cross section is inversely proportional to the laser field intensity in the present intensity range. The two-photon ionization cross section at a higher field intensity may be estimated by extrapolation using this relation. In a previous theoretical study, the two-photon cross section, 6×10^{-51} cm^4 s, was obtained at 1×10^{13} W/cm^2 by using the R-matrix Floquet approach [16]. By extrapolation, we obtain $15(3) \times 10^{-51}$ cm^4 at this field intensity, which agrees with the theoretical value within a factor of $\sim$2.5. Recently, a smaller experimental value, $2.3(7) \times 10^{-51}$ cm^4, was reported by ion-mass spectrometry using FEL [6]. The origin of the large discrepancy from the present value is not clear, but it is partly attributed to the temporal integration factors $T^{(1)}$ and $T^{(2)}$ omitted in the previous study.

IV. EUV-UV TWO-COLOR TWO-PHOTON IONIZATION

Nonresonant two-color two-photon ionization of He [Fig. 1(c)] was studied by using FEL (59.7 nm, 20.8 eV, 1.6×10^{13} W/cm^2) and UV laser (268 nm, 4.63 eV, 1.4×10^{13} W/cm^2) pulses. Figure 3(a) shows averaged photoelectron spectra recorded at $\Delta t = 0$ ps. Photoelectron peaks at 5 and 16.5 eV are due to one-photon and two-photon ionization of Ar and He by FEL, respectively, as observed in the one-color experiments in the previous section. In addition, two peaks are identified at 0.6 and 1.3 eV. From the energy conservation, the peak at 0.6 eV is assigned to photoelectrons produced by nonresonant EUV-UV two-photon ionization of He. When the UV pulse is delayed from the FEL pulse ($\Delta t = +1.3$ ps), this peak at 0.6 eV vanishes as expected for a nonresonant two-photon process [see Fig. 3(b)].

Interestingly, the energy of the other peak at 1.3 eV corresponds to resonant two-color two-photon ionization via

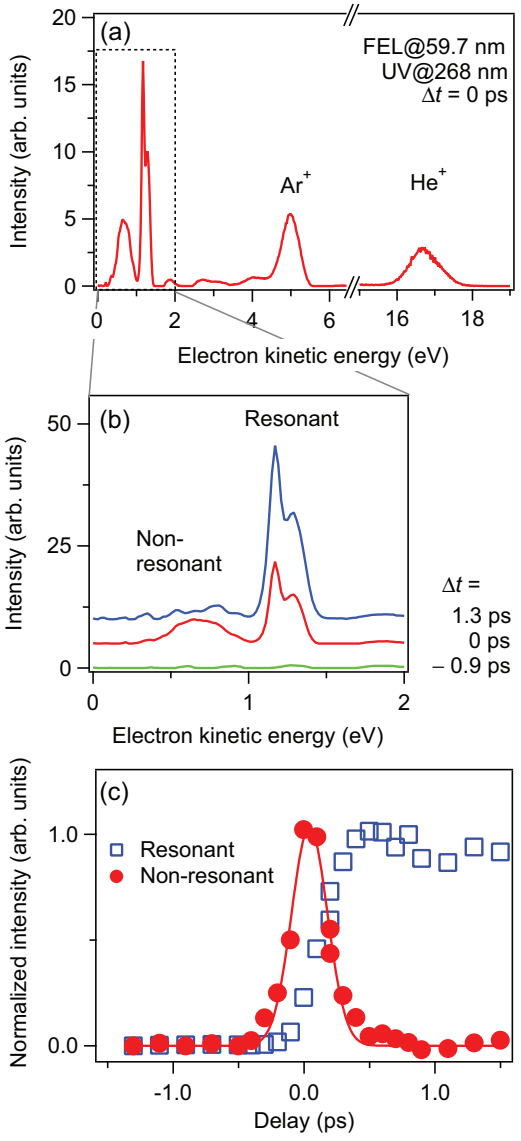

FIG. 3. (Color online) (a) Averaged photoelectron spectra of He-Ar gas mixture using EUV-FEL (20.8 eV, 1.6×10^{13} W/cm^2) and UV laser (4.63 eV, 1.4×10^{13} W/cm^2) pulses at $\Delta t = 0$ ps. The number density ratio between He and Ar is $n^0_{\mathrm{Ar}}/n^0_{\mathrm{He}} = 1.2 \times 10^{-4}$. Two peaks seen at 0.6 and 1.3 eV are assigned to nonresonant and resonant two-color two-photon ionization of He, respectively. (b) Temporal evolution of photoelectron spectra of resonant and nonresonant two-color two-photon ionization of He. (c) Photoelectron signal intensities of He^+ for nonresonant (filled circles) and resonant (open squares) components as a function of the time delay between the FEL (20.8 eV) and UV laser (4.63 eV) pulses. The FWHM of the cross-correlation trace of the nonresonant trace is obtained to be 0.36(3) ps by fitting the data to a Gaussian function.

the $2\,^1P$ state. Indeed, Fig. 3(b) shows that the peak remains at a longer delay ($\Delta t = +1.3$ ps) confirming that excitation to the nonvirtual state having a finite lifetime is involved in the two-photon ionization. The excitation to the $2\,^1P$ state (21.22 eV) requires a larger photon energy shift (0.4 eV) than the fluctuation width (~0.13 eV) [17,21] of the FEL pulse at 59.7 nm (20.8 eV). For such a large energy shift, the laser intensity is so small ($<10^{-3}$) according to the FEL spectra under the present conditions that the one-color two-photon ionization hardly occurs despite the enhancement by the resonance. Accordingly, no signal was identified at the corresponding energy (17.9 eV) in Fig. 3(a). Once the $2\,^1P$ state is populated, however, the intense UV pulse can efficiently ionize the excited He atom by single-photon absorption, producing the photoelectron peak at 1.3 eV.

The intensities of these two photoelectron peaks are plotted as a function of the delay in Fig. 3(c). The intensity of the resonant component (open squares) increases until $\Delta t =$ 0.4 ps and stays almost constant up to $\Delta t = 1.5$ ps, which is consistent with the lifetime (560 ps) of the $2\,^1P$ state [34]. In contrast, the nonresonant signal (filled circles) is peaked at $\Delta t = 0$ ps. The FWHM of the latter is determined to be 0.36(3) ps by a least-squares fitting to a Gaussian function. Since both FEL and UV laser-pulse durations are about 100 fs, the net timing jitter is estimated to be 0.33(3) ps, when a Gaussian envelope is assumed for each pulse.

In the following, we discuss the effect of the timing jitter more in detail by shot-by-shot analysis of the photoelectron spectra. Figure 4(a) shows the distribution of the nonresonant signal intensity, plotted against the FEL intensity for each laser shot. The nominal pulse delay was set to $\Delta t = 0$ ps. The observed map shows a dense distribution on the left, indicating that the nonresonant photoelectron signal is not observed in most of the laser shots by the lack of the temporal overlap between the FEL and UV laser pulses. Figure 4(a) also shows that the distribution extends to a higher signal region by the (partial) temporal overlap between the FEL and UV laser pulses, to form a clear edge along a straight line, as expected from the linear scaling of the nonresonant process against the FEL intensity [see Eq. (4)]. The intensity and temporal fluctuation of FEL both result in a broad distribution of the nonresonant signal intensity as shown in the histogram in Fig. 4(b).

To discuss the observed signal distribution more quantitatively, the time integral in Eq. (3) was simulated using fluctuating FEL pulses $f_{\mathrm{EUV}}(t)$ generated by the partial-coherence method [26] (see Sec. III),

$$T^{(2)}_{\mathrm{EUV,UV}}(\delta) = \int_{-\infty}^{+\infty} f_{\mathrm{EUV}}(t) f_{\mathrm{UV}}(t-\delta) dt, \qquad (8)$$

where δ represents the timing jitter of each FEL pulse.

First we discuss the case free from the timing jitter ($\delta = 0$). Figure 4(c) shows the distribution of the simulated time integral $T^{(2)}_{\mathrm{EUV,UV}}(0)$, normalized by the time integral calculated for the averaged pulse $\bar{f}_{\mathrm{EUV}}(t)$,

$$\bar{T}^{(2)}_{\mathrm{EUV,UV}}(0) = \int_{-\infty}^{+\infty} \bar{f}_{\mathrm{EUV}}(t) f_{\mathrm{UV}}(t) dt. \qquad (9)$$

The obtained distribution shows a clear peak at $T^{(2)}_{\mathrm{EUV,UV}}(0) \sim 1$ as expected, where the distribution width is due to the intensity fluctuation of the FEL pulse.

Now the effect of the timing jitter is investigated by introducing the time-delay δ between the FEL and UV laser pulses. Here δ is chosen randomly for each FEL pulse to reproduce the Gaussian distribution (0.33 ps FWHM) for the timing jitter. The obtained histogram in Fig. 4(d) shows a

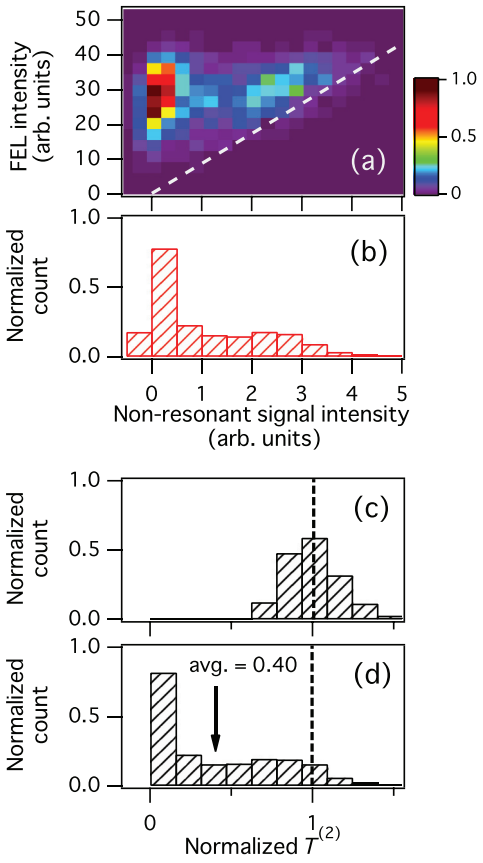

FIG. 4. (Color online) (a) Distribution of nonresonant two-color two-photon ionization of He. The nonzero signal by the temporal overlap of EUV and UV pulses is well explained by a linear function of the EUV-FEL pulse intensity. (b) Distribution of nonresonant signal intensity obtained by the shot-by-shot analysis of the photoelectron spectra at $\Delta t = 0$ ps in Fig. 3(a). (c) Distribution of the normalized $T^{(2)}$ at $\Delta t = 0$ ps simulated for jitter-free FEL pulses. (d) Same as (c), but including the timing jitter of 0.33 ps (FWHM).

broad signal distribution with a sharp peak at around zero, in agreement with the experimental distribution in Fig. 4(b).

Because of the broad distribution, the average of the normalized time integral $T^{(2)}_{\mathrm{EUV,UV}}$ in Fig. 4(d) is only 0.40 compared with $T^{(2)}_{\mathrm{EUV,UV}}(0)(=1)$ for the perfect overlap between the FEL and UV laser pulses without the jitter [see Fig. 4(c)]. Therefore, the observed average-signal intensity needs to be corrected by this factor to estimate the nonresonant two-photon cross section free from the timing jitter. The jitter-free signal ratio, $S^{(2)}_{\mathrm{He^+,NR}}/S^{(1)}_{\mathrm{Ar^+}}$, is estimated to be 1.6(2) from the integrated intensity of the peak at 0.6 eV for the nonresonant component in Fig. 3 ($\Delta t = 0$ ps) (divided by a factor of 0.40), and that for $\mathrm{Ar^+}$ after the saturation correction. Using $n^0_{\mathrm{Ar}}/n^0_{\mathrm{He}} = 1.2 \times 10^{-4}$, $T^{(1)}_{\mathrm{EUV}}/T^{(2)}_{\mathrm{EUV,UV}}(0) = 1.4$, $I_{0,\mathrm{UV}} = 1.4 \times 10^{13}$ W/cm^2, and $\sigma^{(1)}_{\mathrm{Ar}}(20.8\ \mathrm{eV}) = 3.61 \times 10^{-17}$ cm^2 [27], we obtain a jitter-free cross section for nonresonant two-color two-photon ionization of He, $\sigma^{(2)}_{\mathrm{He}}(20.8\ \mathrm{eV},\ 4.63\ \mathrm{eV}) = 4.1(6) \times 10^{-52}$ cm^4 s, from Eq. (7). It should be noted that without the timing-jitter correction, we obtain a significantly smaller value, $1.6(3) \times 10^{-52}$ cm^4 s. This demonstrates that the single-shot analysis of photoelectron spectra allows us to make precise measurements of nonresonant two-color two-photon cross section by accounting for the jitter, showing its advantage over ion-mass spectrometry or conventional photoelectron spectroscopy.

V. SUMMARY

Single-shot photoelectron spectroscopy was employed to study nonresonant two-color two-photon ionization of He at 59.7 and 268 nm using ultrashort FEL and UV laser pulses. The photoelectron spectroscopy allows us to separate contributions from the nonresonant and the resonant ionization via the $2\ ^1P$ state, populated by the wavelength fluctuation of SASE FEL. The temporal evolution of the nonresonant component recorded as a function of the pump and probe time delay, the time resolution was determined to be 0.36(3) ps, which was mainly limited by the timing jitter between the FEL and UV pulses. The shot-by-shot analysis of the photoelectron spectra allows us to determine the absolute cross section for the nonresonant two-color two-photon ionization, $\sigma^{(2)}_{\mathrm{He}}(20.8\ \mathrm{eV}, 4.63\ \mathrm{eV}) = 4.1(6) \times 10^{-52}$ cm^4 s, demonstrating the advantage of the present method for single-shot photoelectron spectroscopy using SASE FEL. The cross section for one-color two-photon ionization of He at the $2\ ^1P$-$1\ ^1S$ resonance photon energy was obtained as $\sigma^{(2)}_{\mathrm{He}}\ (21.2\ \mathrm{eV}, 21.2\ \mathrm{eV}) = 5(1) \times 10^{-50}$ cm^4 s at the EUV field intensity of 3×10^{12} W/cm^2. The absolute cross sections of nonlinear processes should provide a basic understanding of laser-electron interactions in atoms in high-frequency intense laser fields.

ACKNOWLEDGMENTS

The authors are grateful to the SCSS Test Accelerator Operation Group at RIKEN for continuous support in the course of the study. Y.H. and A.H. thank Yamada Science Foundation for financial support. Y.H. acknowledges support from JSPS KAKENHI (Grant No. 24540425). This work was performed with the approval of the SCSS Test Accelerator Operation and Utilization Committee.

[1] M. Yabashi, H. Tanaka, T. Tanaka, H. Tomizawa, T. Togashi, M. Nagasono, T. Ishikawa, J. R. Harries, Y. Hikosaka, A. Hishikawa *et al.*, J. Phys. B **46**, 164001 (2013).

[2] J. Feldhaus, M. Krikunova, M. Meyer, T. Möller, R. Moshammer, A. Rudenko, T. Tschentscher, and J. Ullrich, J. Phys. B **46**, 164002 (2013).

[3] C. Bostedt, J. D. Bozek, P. H. Bucksbaum, R. N. Coffee, J. B. Hastings, Z. Huang, R. W. Lee, S. Schorb, J. N. Corlett, P. Denes *et al.*, J. Phys. B **46**, 164003 (2013).

[4] R. Mitzner, A. A. Sorokin, B. Siemer, S. Roling, M. Rutkowski, H. Zacharias, M. Neeb, T. Noll, F. Siewert, W. Eberhardt *et al.*, Phys. Rev. A **80**, 025402 (2009).

[5] R. Moshammer, T. Pfeifer, A. Rudenko, Y. H. Jiang, L. Foucar, M. Kurka, K. U. Kühnel, C. D. Schröter, J. Ullrich, O. Herrwerth *et al*., Opt. Express **19**, 21698 (2011).
[6] T. Sato, A. Iwasaki, K. Ishibashi, T. Okino, K. Yamanouchi, J. Adachi, A. Yagishita, H. Yazawa, F. Kannari, M. Aoyma *et al*., J. Phys. B **44**, 161001 (2011).
[7] H. Hasegawa, E. J. Takahashi, Y. Nabekawa, K. L. Ishikawa, and K. Midorikawa, Phys. Rev. A **71**, 023407 (2005).
[8] A. Kosuge, T. Sekikawa, X. Zhou, T. Kanai, S. Adachi, and S. Watanabe, Phys. Rev. Lett. **97**, 263901 (2006).
[9] N. Miyamoto, M. Kamei, D. Yoshitomi, T. Kanai, T. Sekikawa, T. Nakajima, and S. Watanabe, Phys. Rev. Lett. **93**, 083903 (2004).
[10] T. Nakajima and L. A. A. Nikolopoulos, Phys. Rev. A **66**, 041402 (2002).
[11] L. A. A. Nikolopoulos and P. Lambropoulos, J. Phys. B **34**, 545 (2001).
[12] D. Proulx and R. Shakeshaft, J. Phys. B **26**, L7 (1993).
[13] J. Purvis, M. Dörr, M. Terao-Dunseath, C. J. Joachain, P. G. Burke, and C. J. Noble, Phys. Rev. Lett. **71**, 3943 (1993).
[14] A. Saenz and P. Lambropoulos, J. Phys. B **32**, 5629 (1999).
[15] T. Sako, J. Adachi, A. Yagishita, M. Yabashi, T. Tanaka, M. Nagasono, and T. Ishikawa, Phys. Rev. A **84**, 053419 (2011).
[16] H. W. van der Hart and P. Bingham, J. Phys. B **38**, 207 (2005).
[17] Y. Hikosaka, M. Fushitani, A. Matsuda, C. M. Tseng, A. Hishikawa, E. Shigemasa, M. Nagasono, K. Tono, T. Togashi, H. Ohashi *et al*., Phys. Rev. Lett. **105**, 133001 (2010).
[18] A. Hishikawa, M. Fushitani, Y. Hikosaka, A. Matsuda, C.-N. Liu, T. Morishita, E. Shigemasa, M. Nagasono, K. Tono, T. Togashi *et al*., Phys. Rev. Lett. **107**, 243003 (2011).
[19] Y. Hikosaka, M. Fushitani, A. Matsuda, T. Endo, Y. Toida, E. Shigemasa, M. Nagasono, K. Tono, T. Togashi, M. Yabashi *et al*., Phys. Rev. A **88**, 023421 (2013).
[20] C.-N. Liu, A. Hishikawa, and T. Morishita, Phys. Rev. A **86**, 053426 (2012).
[21] T. Shintake, H. Tanaka, T. Hara, T. Tanaka, K. Togawa, M. Yabashi, Y. Otake, Y. Asano, T. Bizen, T. Fukui *et al*., Nat. Photon. **2**, 555 (2008).
[22] A. A. Wills, A. A. Cafolla, and J. Comer, J. Phys. B **24**, 3989 (1991).
[23] T. X. Carroll, J. D. Bozek, E. Kukk, V. Myrseth, L. J. Saethre, T. D. Thomas, and K. Wiesner, J. Electron Spectrosc. Relat. Phenom. **125**, 127 (2002).
[24] A. l'Huillier, L. A. Lompre, G. Mainfray, and C. Manus, Phys. Rev. A **27**, 2503 (1983).
[25] L. A. A. Nikolopoulos and P. Lambropoulos, Phys. Rev. A **74**, 063410 (2006).
[26] T. Pfeifer, Y. H. Jiang, S. Düsterer, R. Moshammer, and J. Ullrich, Opt. Lett. **35**, 3441 (2010).
[27] W. F. Chan, G. Cooper, X. Guo, G. R. Burton, and C. E. Brion, Phys. Rev. A **46**, 149 (1992).